Electronic Supplementary Material (ESI) for Nanoscale.


**Growth and Nanomechanical Characterization of Nanoscale 3D Architectures Grown Via Focused Electron Beam Induced Deposition (Supplement)**

1. **Compression Tests**

   See videos (1_5_Ratio.mp4 and 1_3_Ratio.mp4) for both pillars depicted in figure 2 of the main text.

2. **Cantilever Bend Flexural tests**

   See video (Cantilever_test.mp4) for the data depicted in Figure 3 of the main text.

3. **3D Architecture Displacement Tests**

   See videos (TowerInitial.mp4, Tower_Fatigue.mp4, and Pyramid_fatigue.mp4) for both the pyramidal and tower compression tests as depicted in Figure 6 of the main text.

4. **ALD Coating Modulus**

   The conformal ceramic coating has the effect of increasing the modulus of the pillars. The effective elastic modulus is related to the material moduli by:

$$E_{eff} = f \cdot E_{Al_2O_3} + (1 - f) \cdot E_{PtC_x} \quad (1)$$

where f is the cross-sectional area fraction of the two materials, in this case:

$$f = \frac{A_{Al_2O_3}}{A_{PtC_x} + A_{Al_2O_3}} \quad (2)$$

Using equations 1 and 2 and estimating the modulus of the FEBID material ($E_{PtCx}$) to be the average value of 9.7 GPa, the average modulus of the alumina thin film coating was calculated to be approximately 58 GPa. The film thickness was determined using reflectometry. Five separate measurements were made using a Filmetrics F20-UV reflectometer. The film thickness ranged from 11 nm to 13 nm with a 99% goodness of fit for the spectral data. Typical values of modulus for high quality ALD alumina thin films are 164 $\pm$ 15 GPa.[1] In general, high quality alumina films are typically grown in excess of 300 $^{o}$C and significant reduction in quality can occur in films grown at lower temperatures.[2, 3] In our case, the quality of the film likely suffers due to the low temperature (100 $^{o}$C) used to the preservation of the three-dimensional structure. Additionally, it is possible that the FEBID structure is not well-adhered to the $Al_2O_3$ coating and bearing a disproportionate fraction of the load.

## 5. Electrical Measurements on Suspended Nanowires

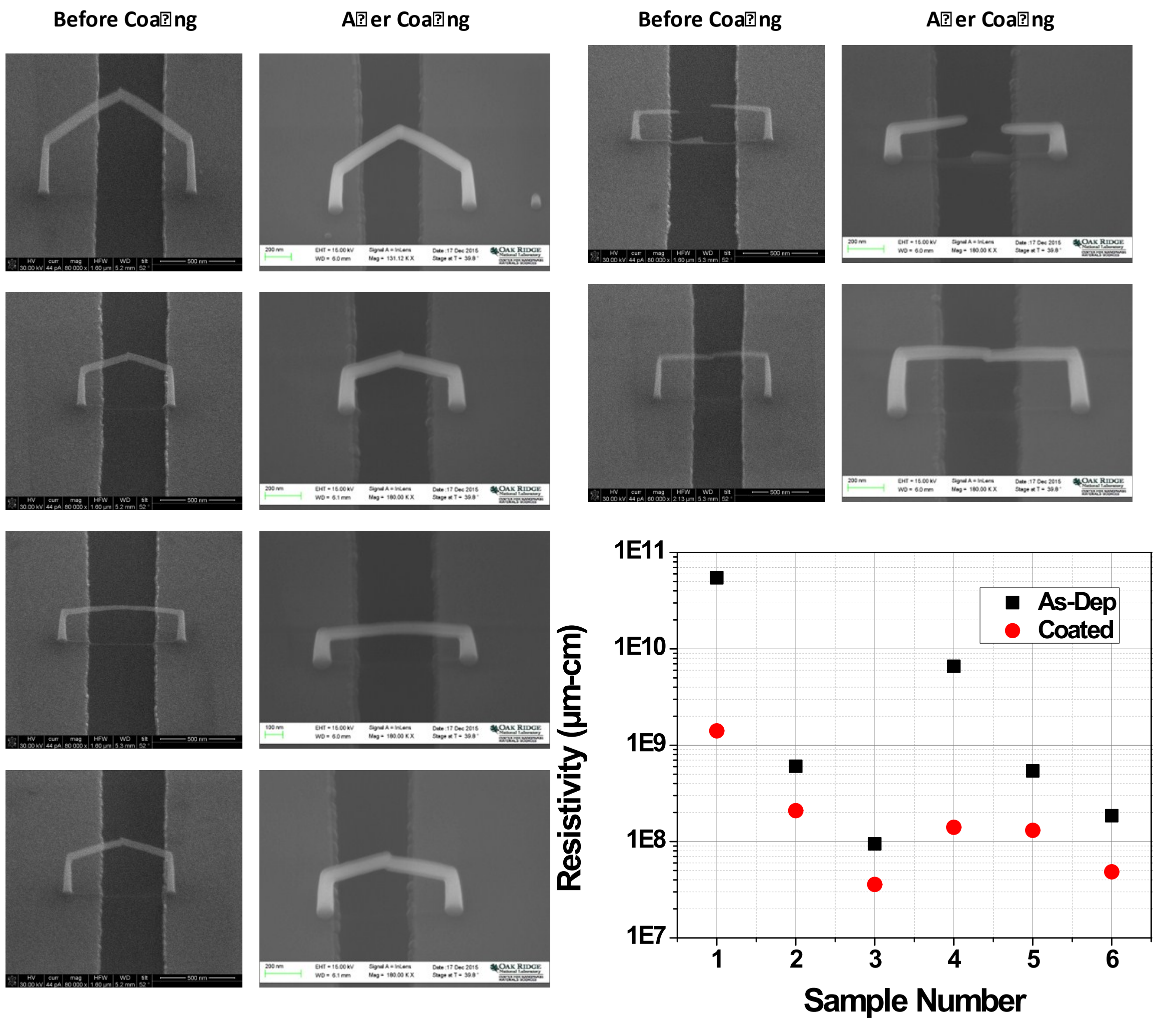


**S 1:** Images both before and after coating with ALD $Al_2O_3$ of the suspend nanowires. The images to the right show nanowires that did not fully connect over the gap between the electrodes (represented by sample number 1 and 4 in the plot below). For the resistivity calculations, the cross-sectional area was approximated assuming a rectangular shape and measuring directly from tilted and top-down SEM images. In the main body of the text samples 1 and 4 are omitted, but are included here to illustrate the effect that co-deposition can have. In sample 4, the gap between the two arms of the nanowire was small enough that after ALD the gap was closed. This is also reflected in the lower resistivity of the coated sample number 4.

## 6. Simulation Results

The commercial finite element software package, COMSOL™ Multiphysics, was used to simulate the stress distribution of the truss structures. The structures were modeled as a simple isotropic linear elastic material with a modulus of 10 GPa, a Poisson's ratio of 0.22, and a density of 4.55 g/cm$^3$. For simplicity, the individual elements of the truss structures were modeled as rectangles with lengths and widths as measured from experiment.

The von Mises stress distribution in the nanoarchitectures was calculated assuming compressive load of 0.015 mN is applied to both geometries. The load was applied in the negative z-direction from the top of the structure and fixed constraint is placed at the bottom of the structure. The von Mises stress is defined from in terms of the second deviatoric stress invariant ($J_2$),

$$\sigma_{VM} = \sqrt{3J_2} \qquad (1)$$

which is defined in terms of the Cauchy stress tensor,

$$\sigma = \begin{bmatrix} \sigma_{11} & \sigma_{12} & \sigma_{13} \\ \cdot & \sigma_{22} & \sigma_{23} \\ \cdot & \cdot & \sigma_{33} \end{bmatrix} \qquad (2)$$

as:

$$J_2 = \frac{1}{6}\left((\sigma_{11} - \sigma_{22})^2 + (\sigma_{22} - \sigma_{33})^2 + (\sigma_{33} - \sigma_{11})^2\right) + \sigma_{12}^2 + \sigma_{23}^2 + \sigma_{13}^2 \qquad (5)$$

The von Mises yield criterion for yielding states that the material will yield if the stress exceeds that of the von Mises stress. After the von Mises stress was calculated, the values were normalized to a scale of 0 to 1; taking 1 to be the maximum calculated von Mises stress for each structure. The two structures were normalized on separate scales. The maximum value for the tower structure was ~16 times smaller than that of the pyramidal structure.

## 7. Viscoelasticity

The slopes of the loading/unloading curves in section **Figure 2**, and **Figure 5** and the observed hysteresis and strain recovery in **Figure 6** of the main text indicates that the deformation is viscoelastic in nature. To explore further, four separate constant displacement tests of varying displacement rates were performed on a tower truss structure. The displacement depth was limited to 100 nm in order to stay in region I as identified in **Figure 6c**. The constant displacement rate used in during each separate test was cycled in ascending order from 1 nm/s to 8 nm/s. The results of this test are depicted in S2. Part **a** shows the load plotted as a function of displacement and part **b** shows the load plotted as a function of time for the same tests. The viscoelastic behavior of the truss structures is clearly depicted in the strong dependence of apparent elasticity on the strain rate during deformation. This viscoelasticity likely originates in the polymeric nature[4] of the carbonaceous matrix of the FEBID material. Future studies will investigate the viscoelastic properties of the material in more detail.

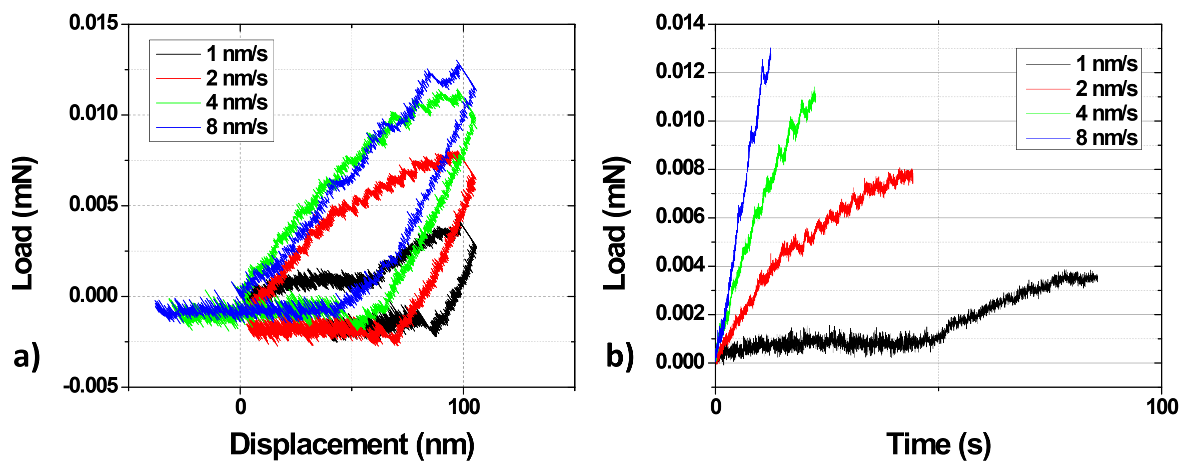


**S 2:** a) Load vs. displacement curves resulting from the deformation of a tower truss structure during constant displacement tests with rates indicated in the legend. b) Load vs. time curves corresponding to the same tests as shown in a).


1. M. Berdova, T. Ylitalo, I. Kassamakov, J. Heino, P. T. Törmä, L. Kilpi, H. Ronkainen, J. Koskinen, E. Hæggström and S. Franssila, *Acta Materialia*, 2014, **66**, 370-377.
2. M. D. Groner, F. H. Fabreguette, J. W. Elam and S. M. George, *Chemistry of Materials*, 2004, **16**, 639-645.
3. O. M. E. Ylivaara, X. Liu, L. Kilpi, J. Lyytinen, D. Schneider, M. Laitinen, J. Julin, S. Ali, S. Sintonen, M. Berdova, E. Haimi, T. Sajavaara, H. Ronkainen, H. Lipsanen, J. Koskinen, S.-P. Hannula and R. L. Puurunen, *Thin Solid Films*, 2014, **552**, 124-135.

4. W. Ding, D. A. Dikin, X. Chen, R. D. Piner, R. S. Ruoff, E. Zussman, X. Wang and X. Li, *Journal of Applied Physics*, 2005, **98**, 014905.